MPP-2012-149

High-resolution supernova neutrino spectra represented by a simple fit

Irene Tamborra,[1] Bernhard Müller,[2] Lorenz Hüdepohl,[2] Hans-Thomas Janka,[2] and Georg Raffelt[1]

[1] *Max-Planck-Institut für Physik (Werner-Heisenberg-Institut), Föhringer Ring 6, 80805 München, Germany*
[2] *Max-Planck-Institut für Astrophysik, Karl-Schwarzschild-Str. 1, 85748 Garching, Germany*

(Dated: November 19, 2012)

To study the capabilities of supernova neutrino detectors, the instantaneous spectra are often represented by a quasi-thermal distribution of the form $f_\nu(E) \propto E^\alpha e^{-(\alpha+1)E/E_{\rm av}}$ where $E_{\rm av}$ is the average energy and α a numerical parameter. Based on a spherically symmetric SN model with full Boltzmann neutrino transport we have, at a few representative post-bounce times, re-converged the models with vastly increased energy resolution to test the fit quality. For our examples, the spectra are well represented by such a fit in the sense that the counting rates for a broad range of target nuclei, sensitive to different parts of the spectrum, are reproduced very well. Therefore, the first few energy moments of numerical spectra hold enough information to forecast the response of multi-channel supernova neutrino detection.

PACS numbers: 14.60.Pq, 97.60.Bw

I. INTRODUCTION

The neutrino signal from the next nearby core-collapse supernova (SN) remains the most coveted target for low-energy neutrino astronomy. Galactic SNe are rare, perhaps a few per century, and such an observation will be a once-in-a-lifetime opportunity to look deeply inside a collapsing star and learn about its astrophysical workings as well as about neutrino properties. Several detectors worldwide are in operation that will register a high-statistics signal while others are in preparation or under discussion [1].

In order to assess the physics potential of various detectors or detection principles one needs the expected flavor-dependent SN neutrino flux spectra. In the absence of self-consistent three-dimensional core-collapse simulations there is no standard SN neutrino flux model and moreover, the flavor-dependent flux spectra depend on the properties of the incompletely known neutron-star equation of state, on the properties of the collapsing star, notably its mass, and, of course, on time for any given case. In this situation parametric studies, taking account of the plausible range of predictions, are the preferred course of action.

We here address one particular aspect of such studies, i.e. the plausible spectral shape of SN neutrino fluxes. On a rough level of approximation, the spectra follow a thermal distribution that can be described in terms of an effective temperature. In detail the spectra formation is a complicated process, different energy groups emerging from different depths in the proto-neutron star atmosphere [3, 5], and a more refined description is necessary for a more detailed understanding.

The next level of sophistication is to describe the non-equilibrium spectra by a three-parameter fit that allows for deviations from a strictly thermal spectrum [4]. One particularly simple realization are spectra where the monochromatic neutrino number flux has the form [5]

$$f_\nu(E) \propto E^\alpha \, e^{-(\alpha+1)E/E_{\rm av}} \, . \qquad (1)$$

Here, $E_{\rm av}$ is the average energy and α a numerical parameter; the value $\alpha = 2$ corresponds to a Maxwell-Boltzmann spectrum. The three parameters $E_{\rm av}$, α, and the overall normalization can be determined, for example, if a numerical SN simulation provides the energy flux (luminosity) L_ν in some flavor, the average energy $E_{\rm av} = \langle E_\nu \rangle$ and some other energy moment, for example $\langle E_\nu^2 \rangle$ or sometimes $\langle E_\nu^3 \rangle$.

While spectra of the form of Eq. (1) certainly provide a reasonable overall representation, it is not obvious how well the spectral tails are reproduced. This question can be of interest for the study of detector responses with target nuclei with a significant energy threshold, for example lead in the Halo detector, argon in future large-scale liquid argon detectors, or subdominant detection channels on oxygen in water Cherenkov detectors or carbon in scintillator detectors.

Modern numerical SN codes treat neutrino transport with Boltzmann solvers that are expected to produce physically accurate spectra. On the other hand, neutrino transport is the most CPU-time consuming aspect of SN simulations so that in practice the energy resolution is limited. For example, in typical simulations of the Garching group, 17–21 energy bins are used and they do not resolve the spectral tails very well.

In order to study the spectral shape and its impact on the relative detector response of different materials we have produced better resolved spectra at a few representative post-bounce times of a representative spherically symmetric simulation by re-converging models at a given post-bounce time after refining the energy binning. With these high-resolution spectra we can then test how well a global fit of the form of Eq. (1) reproduces the relative neutrino counting rates of different materials that probe rather different parts of the spectrum.

To this end we describe in Sec. II our numerical SN model and in Sec. III the target materials. A comparison between counting rates based on the numerical spectra and the fitted ones is performed in Sec. IV before concluding in Sec. V.

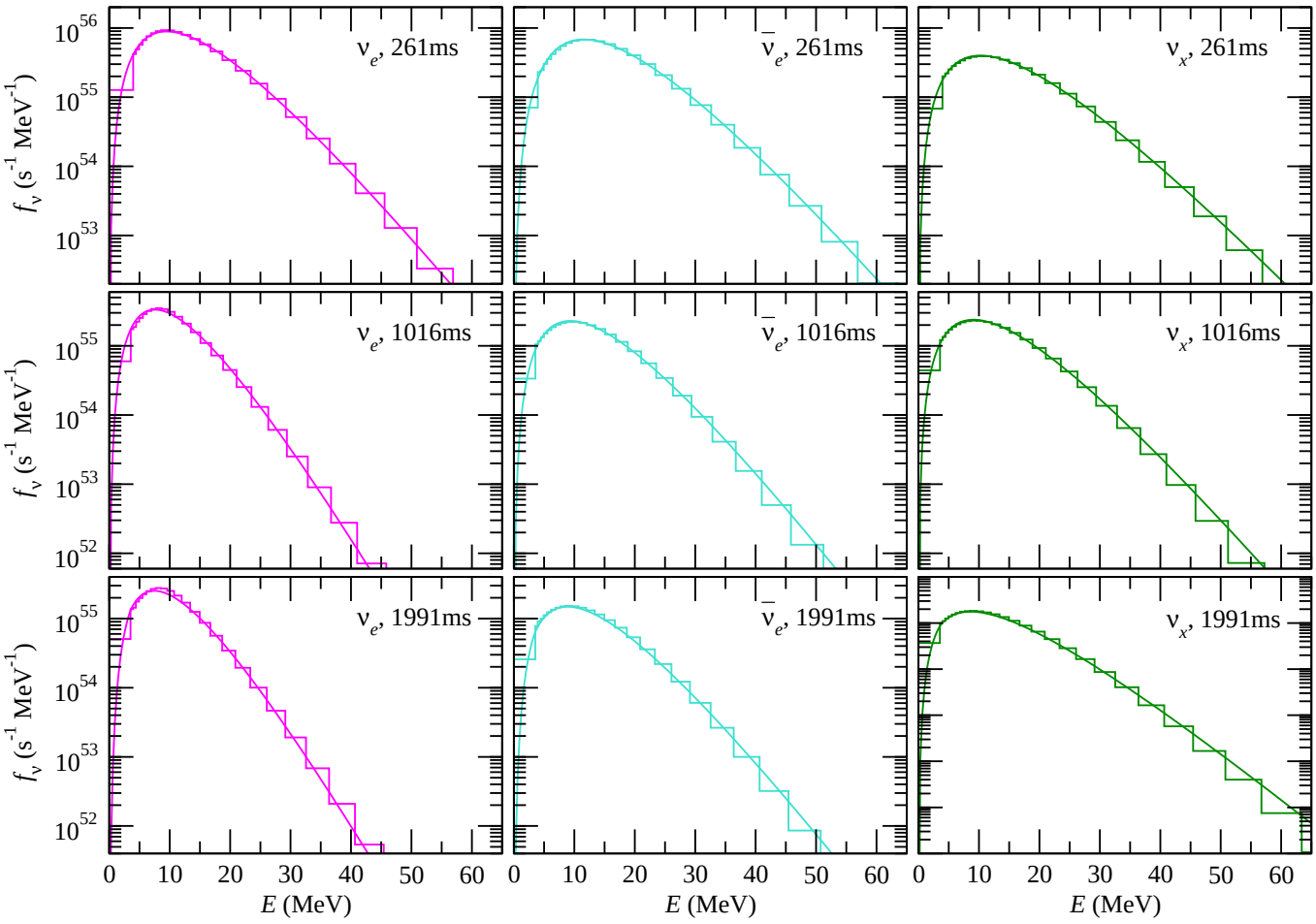

FIG. 1: Spectra for species ν_e (left column), $\bar{\nu}_e$ (middle column) and ν_x (right column) for post-bounce times of 261 ms (top row), 1016 ms (middle row), and 1991 ms (bottom row). The data from the PROMETHEUS-VERTEX HR spectra are shown as step functions, and the continuous curves are quasi-thermal fits according to Eq. (1).

II. NUMERICAL SUPERNOVA MODEL

We have performed simulations of the $15M_\odot$ progenitor of Woosley and Weaver [6] with the neutrino hydrodynamics code PROMETHEUS-VERTEX [7], which solves the 0th and 1st neutrino moment equations with a variable Eddington factor closure that is provided by the formal solution of a simplified (model) Boltzmann equation. The explosion of the spherically symmetric model was artificially initiated 500 ms after bounce. For the dynamical evolution of the model including the feedback into the hydrodynamics, we used 21 energy bins with a typical resolution $\delta\epsilon/\epsilon$ (ratio of zone width to zone mean energy) of ~ 0.29. We refer to this setup as the standard resolution (SR) case.

In order to accurately predict the shape of the neutrino spectra, particularly in the high-energy tail, we computed high-resolution (HR) stationary solutions of the neutrino transport equations for a representative time during the accretion phase (261 ms after bounce) and for the proto-neutron star cooling phase (1016 ms and 1991 ms) using the matter background from the dynamical simulation. Different from the dynamical run, the original treatment of [7] for the Doppler and redshift terms is used instead of that of [8], and the threshold values for the monochromatic neutrino energy density below which a spectral extrapolation is performed has been reduced by a factor of 100. We also transition continuously from the comoving frame to the lab frame once neutrino interactions cease in order to eliminate artifacts due to the velocity jump in the shock. These numerical changes accelerate convergence and help to obtain smoother and more accurate spectra.

The spacing of the logarithmic energy grid was much finer with 42 bins and $\delta\epsilon/\epsilon = 0.11$ in the HR case. For better comparison, the stationary solutions for the SR case were re-computed with precisely the same numerics. Figure 1 shows the obtained HR spectra for the species ν_e, $\bar{\nu}_e$, and ν_x, where the latter stands for any of ν_μ, $\bar{\nu}_\mu$, ν_τ or $\bar{\nu}_\tau$.

In order to compare the numerical spectra (histograms) with a quasi-thermal fit of the form of Eq. (1),

TABLE I: Fit parameters α, luminosities L_ν, and neutrino mean energies $\langle E_\nu \rangle$ for different neutrino species and post-bounce times for HR and SR spectra.

t [ms]	species	$\alpha_{\rm HR}$	$\alpha_{\rm SR}$	$L_{\nu,{\rm HR}}$ [10^{52} erg s^{-1}]	$L_{\nu,{\rm SR}}$ [10^{52} erg s^{-1}]	$\langle E_\nu \rangle_{\rm HR}$ [MeV]	$\langle E_\nu \rangle_{\rm SR}$ [MeV]
261	ν_e	2.6458	2.7346	2.8040	2.6808	13.0518	12.8673
261	$\bar{\nu}_e$	3.1263	3.2291	2.7983	2.7059	15.2272	15.0460
261	ν_x	2.4245	2.4822	1.5836	1.6283	14.4851	14.4845
1016	ν_e	2.9054	3.1370	0.6186	0.6251	10.1385	10.2777
1016	$\bar{\nu}_e$	2.7812	2.8814	0.6750	0.7035	12.6864	12.8686
1016	ν_x	2.3917	2.5159	0.7525	0.7684	12.8957	13.0033
1991	ν_e	2.9226	3.1724	0.4813	0.4726	10.0103	10.0095
1991	$\bar{\nu}_e$	2.6107	2.6679	0.4389	0.4429	12.2790	12.3657
1991	ν_x	2.3444	2.4889	0.5383	0.5501	12.3097	12.3869

we determine the parameter α in terms of the energy moments of the distribution. One way of fixing α is to use the energy moment of order k and notice that

$$\frac{\langle E_\nu^k \rangle}{\langle E_\nu^{k-1} \rangle} = \frac{k+\alpha}{1+\alpha} \langle E_\nu \rangle \,. \tag{2}$$

We have checked that for our cases the implied value of α does not strongly depend on k, which already implies that this type of fit is a reasonable representation. In the following we will use $k = 2$, i.e., the relation

$$\frac{\langle E_\nu^2 \rangle}{\langle E_\nu \rangle^2} = \frac{2+\alpha}{1+\alpha} \,. \tag{3}$$

We show examples of the fits as continuous curves both on a logarithmic and on a linear scale in Figs. 1 and 2, respectively, and find that visually the fits work very well. Values for the fit parameter α, the luminosity L_ν, and the neutrino mean energy $\langle E_\nu \rangle$ for the three snapshots and for the different neutrino species ν_e, $\bar{\nu}_e$, and ν_x are listed in Table I both for the HR and the SR case. We note that despite the lower energy resolution, the SR spectra from the dynamical simulation typically give very similar luminosities and mean energies, which are consistent with the HR case within $\sim 5\%$ or less. The fit parameter α agrees similarly well except for ν_e in the post-explosion phase with a deviation of up to 9%. However, this is due to a very steep dependence of α on the second energy moment, $\langle E_\nu^2 \rangle$, when the energy ratio in Eq. (3) is close to unity, and does not affect the fit curves appreciably.

III. DETECTION CROSS SECTIONS

In existing detectors, SN neutrinos are primarily measured in the $\bar{\nu}_e$ channel by virtue of the inverse beta decay (IBD) reaction $\bar{\nu}_e + p \to n + e^+$. The cross section varies roughly as E_ν^2 so that the overall event rate is well reproduced, if the SN neutrino spectrum is approximated by a quasi-thermal spectrum where the second energy moment is used to determine α.

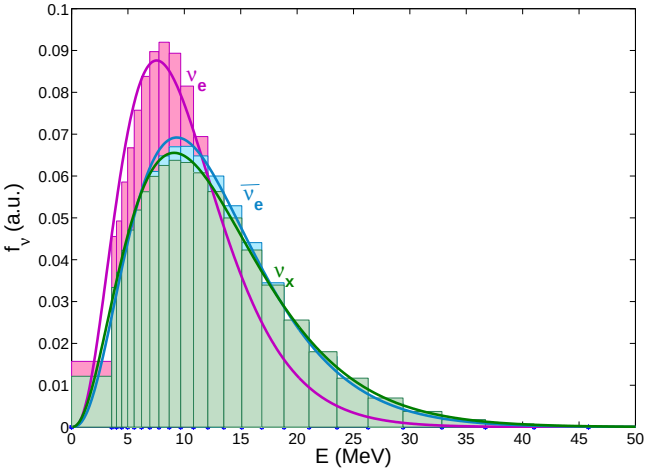

FIG. 2: Spectra for species ν_e, $\bar{\nu}_e$ and ν_x. Histograms are the PROMETHEUS-VERTEX HR spectra of our model at time 1016 ms. The continuous curves are quasi-thermal fits according to Eq. (1).

However, other detection channels are also of interest. One is elastic scattering on electrons where the cross section varies roughly linearly with E_ν. Of greater interest for our study are reactions with a higher energy threshold or steeper energy variation than IBD. One example is the recently built HALO detector in SNOLAB where 79 tons of lead are used as target material. Other examples are reactions on argon in future liquid argon detectors that are primarily considered in the context of long-baseline neutrino oscillation studies and reactions on oxygen in water Cherenkov detectors and on carbon in liquid scintillator detectors.

In our study we consider several selected reactions that span a broad range of spectral responses to neutrino fluxes and show the energy-dependent cross sections in Fig. 3. The reaction sensitive to the lowest range of energies is elastic scattering on electrons via both CC and NC for ν_e and $\bar{\nu}_e$ and via NC interaction for ν_x [9].

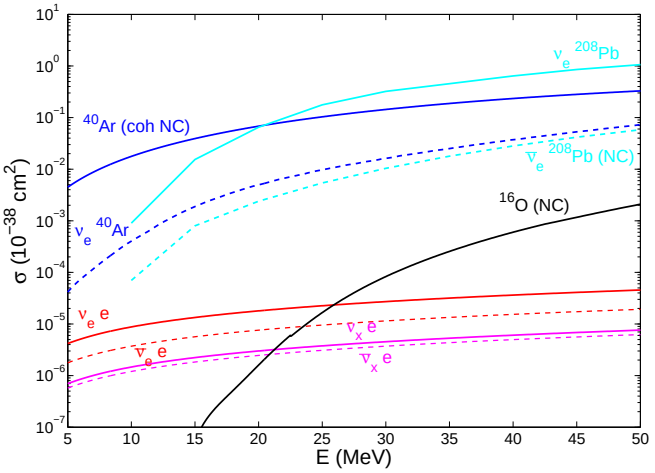

FIG. 3: Neutrino cross sections on some representative target nuclei (see text for details).

In nuclei, CC interactions proceed via $\nu_e + (N,Z) \to (N-1,Z+1) + e^-$ and $\bar{\nu}_e + (N,Z) \to (N+1,Z-1) + e^+$, respectively. The $\bar{\nu}_e$ interaction is typically suppressed at a given energy with respect to the ν_e interaction due to Pauli blocking. Neutral current interactions may also produce observable signals via ejected nucleons or de-excitation photons. As one example we consider NC interactions with ^{16}O [10–13], which is relevant for water-based detectors.

Interactions with heavier nuclei, such as lead, may yield quite high rates of both CC and NC interactions. Observable signatures include leptons and ejected nucleons. Single and multiple neutron ejections are possible. The relevant interactions for lead-based detectors are $\nu_e + {}^A\mathrm{Pb} \to e^- + {}^A\mathrm{Bi}^*$ and $\nu_x + {}^A\mathrm{Pb} \to \nu_x + {}^A\mathrm{Pb}^*$. For both CC and NC cases, the resulting nuclei de-excite via neutron emission. Antineutrino CC interactions are strongly suppressed. Although natural lead contains isotopes other than ^{208}Pb, the neutron cross section for $A = 208$ should be similar to other components. For the Pb cross sections see Refs. [14–17].

Liquid argon detectors will have excellent sensitivity to ν_e via the CC interaction $\nu_e + {}^{40}\mathrm{Ar} \to e^- + {}^{40}\mathrm{K}^*$. This is an interaction for which the de-excitation γs from ^{40}K* can be observed. The reaction $\bar{\nu}_e + {}^{40}\mathrm{Ar} \to e^+ + {}^{40}\mathrm{Cl}^*$ will also occur and can be tagged via the pattern of γs. NC excitations are possible, although little information is available in the literature. Energy thresholds as low as few MeV may be possible. The cross sections are reported in Refs. [18–22].

For the different channels that we consider, we use the cross sections as reported by Scholberg [1]. They have been used in the SNOWGLOBES software package [2].

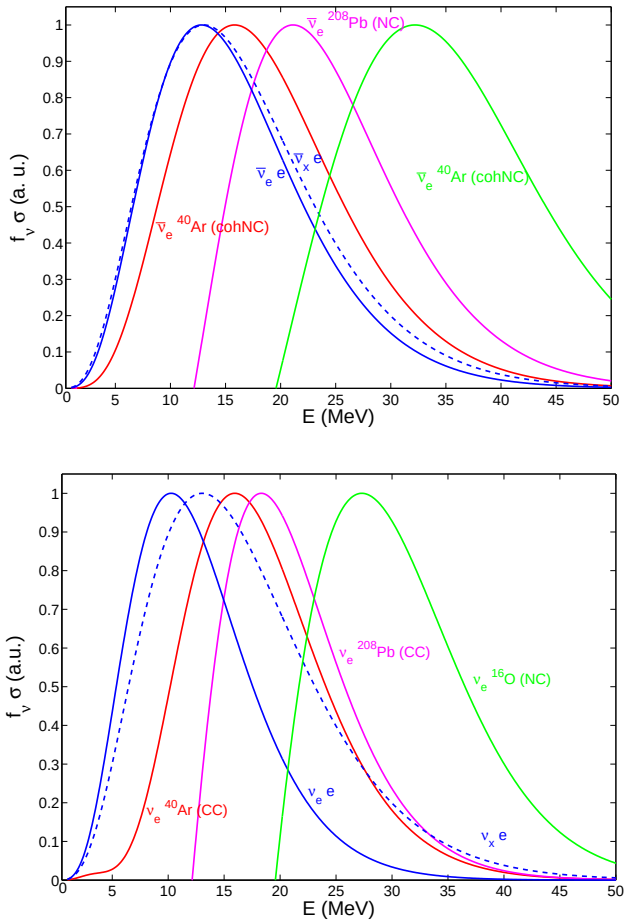

FIG. 4: Detection rate as a function of neutrino energy for different reactions, based on our 1016 ms model. *Top:* Antineutrinos. *Bottom:* Neutrinos.

IV. COUNTING RATES

The detector counting rate as a function of incoming neutrino energy is proportional to $f_\nu(E)\sigma(E)$. Based on the numerical neutrino spectra for the 1016 ms model, we show this quantity in Fig. 4 for our suite of interaction processes, normalized to the same maximum rate. This plot demonstrates that the different detection processes probe vastly different parts of the neutrino spectra.

We now compare the total counting rates for each of our reactions using as a neutrino spectrum either the numerical output directly (rate $N_{\rm num}$) compared with the rate inferred if the spectrum is represented by our fit function (rate $N_{\rm fit}$). In Table II, we report the ratio $N_{\rm fit}/N_{\rm num}$ for neutrinos (top part) and antineutrinos (bottom part). The agreement between $N_{\rm num}$ and $N_{\rm fit}$ is very good and typically the error is only a few percent. Even for the oxygen reaction, which probes the highest-energy tail of all examples, the difference is only some 10–20%. Assuming complete flavor conversions due to neutrino oscillations ($\nu_e \to \nu_x$, and the same for antineutrinos), we tested that the ratio $N_{\rm fit}/N_{\rm num}$ differs from

TABLE II: Ratio of counting rate based on our spectral fit and the direct numerical spectrum, $N_{\rm fit}/N_{\rm num}$.

t[ms]	ν_e ^{40}Ar CC	ν_e ^{208}Pb CC	$\nu_e e$	$\nu_x e$	ν_e ^{16}O NC
261	1.011	1.016	1.005	1.004	1.014
1016	1.019	1.061	1.007	1.004	0.908
1991	1.021	1.072	1.007	1.003	0.901

t[ms]	$\bar{\nu}_e$ ^{40}Ar NC	$\bar{\nu}_e$ ^{208}Pb NC	$\bar{\nu}_e e$	$\bar{\nu}_x e$	$\bar{\nu}_e$ ^{16}O NC
261	1.005	1.018	1.005	1.004	1.051
1016	1.006	1.032	1.005	1.004	1.160
1991	1.006	1.032	1.005	1.003	1.176

the ones reported in Table II only on the level of tenths of a percent (results not shown here). Such a result further confirms the good quality of the alpha-fit.

V. CONCLUSIONS

We have produced high-resolution neutrino spectra at several postbounce times of a spherically symmetric SN simulation and compared the numerical spectra with the analytic fit of Eq. (1), based on the first two energy moments of the numerical distribution. These fitted spectra account well for the detection rates in SN neutrino detectors with vastly different target nuclei. We conclude that for the purpose of signal forecast in different detectors, reasonably good accuracy can be achieved by considering the lowest two energy moments of numerically produced spectra. This insight simplifies parametric studies of detection forecasts for the neutrino signal from the next nearby SN because it is sufficient to represent the non-equilibrium spectra by a simple three-parameter quasi-thermal fit.

Acknowledgments

We acknowledge partial support by the Deutsche Forschungsgemeinschaft under grant TR-7 "Gravitational Wave Astronomy" and the Cluster of Excellence EXC-153 "Origin and Structure of the Universe" and by the European Union Initial Training Network Invisibles PITN-GA-2011-289442. I.T. acknowledges support by the Alexander von Humboldt Foundation.

[1] K. Scholberg, Annu. Rev. Nucl. Part. Sci. **62** (2012) 81. [arXiv:1205.6003].
[2] `http://www.phy.duke.edu/~schol/snowglobes`.
[3] G. G. Raffelt, Astrophys. J. **561** (2001) 890.
[4] H.-T. Janka and W. Hillebrandt, Astron. Astrophys. **224** (1989) 49.
[5] M. T. Keil, G. G. Raffelt and H.-T. Janka, Astrophys. J. **590** (2003) 971.
[6] S. E. Woosley and T. A. Weaver, Astrophys. J. Suppl. **101** (1995) 181.
[7] M. Rampp and H.-T. Janka, Astron. Astrophys. **396** (2002) 361.
[8] B. Müller, H. Dimmelmeier and H.-T. Janka, Astrophys. J. Suppl. **189** (2010) 104.
[9] W. J. Marciano and Z. Parsa, J. Phys. G **29** (2003) 2629.
[10] E. Kolbe, K. Langanke and P. Vogel, Phys. Rev. D **66** (2002) 013007.
[11] W. C. Haxton and C. Johnson, Phys. Rev. Lett. **65** (1990) 1325.
[12] W. C. Haxton, Phys. Rev. C **37** (1988) 2660.
[13] K. Langanke, P. Vogel and E. Kolbe, Phys. Rev. Lett. **76** (1996) 2629.
[14] G. M. Fuller, W. C. Haxton and G. C. McLaughlin, Phys. Rev. D **59** (1999) 085005.
[15] E. Kolbe and K. Langanke, Phys. Rev. C **63** (2001) 025802.
[16] J. Toivanen, E. Kolbe, K. Langanke, G. Martinez-Pinedo and P. Vogel, Nucl. Phys. A **694** (2001) 395.
[17] A. R. Samana and C. A. Bertulani, Phys. Rev. C **78**, 024312 (2008).
[18] R. S. Raghavan, Phys. Rev. D **34** (1986) 2088.
[19] I. Gil Botella and A. Rubbia, JCAP **0310** (2003) 009.
[20] A. Bueno, I. Gil Botella and A. Rubbia, hep-ph/0307222.
[21] I. Gil Botella and A. Rubbia, JCAP **0408** (2004) 001.
[22] M. S. Athar and S. K. Singh, Phys. Lett. B **591** (2004) 69.
[23] J. F. Beacom and M. R. Vagins, Phys. Rev. Lett. **93** (2004) 171101.